ARSENIC RELEASE FROM CHLORINE PROMOTED OXIDATION OF PYRITE IN THE ST. PETER SANDSTONE AQUIFER, EASTERN WISCONSIN

Nicole West

Thesis submitted to the faculty of the Virginia Polytechnic Institute and State University in partial fulfillment of the requirements for the degree of

Master of Science in
Geosciences

Approved

Madeline Schreiber
John Chermak
Don Rimstidt

April 25th, 2008
Blacksburg, VA

Keywords: Arsenic, chlorination, St. Peter Sandstone, Fe-oxides

Arsenic release from chlorine promoted oxidation of pyrite in the St. Peter Sandstone Aquifer, eastern Wisconsin

Nicole West

ABSTRACT

High arsenic concentrations (>100 ppb) have been measured in wells completed in the Ordovician St. Peter sandstone aquifer of eastern Wisconsin. The primary source of arsenic is As-bearing sulfide minerals within the aquifer. There is concern that periodic disinfection of wells by chlorination may facilitate arsenic release to groundwater by increasing the rate of sulfide mineral oxidation. Current guidance from the Wisconsin Department of Natural Resources recommends a "low-dose" treatment of 20% of the chlorine strength and 10% of the of the contact time of chlorine treatments used in non-arsenic impacted wells for well disinfection and biofilm removal. In order to provide information pertaining to WDNR's recommendations, St. Peter sulfide minerals were reacted with a range of chlorine "shock-treatments" similar to those occurring in wells. This study focuses on abiotic processes that mobilize arsenic from the solid phase during controlled exposure to chlorinated solutions.

Thin sections were made from aquifer material collected at Leonard's Michael quarry, located in Winnebago County, Wisconsin. Bulk arsenic content of this material was measured as 674 ppm. Quantitative EPMA analysis shows As zoning in pyrite grains with concentrations up to 1 wt. % As. After mineral characterization, the thin sections were exposed to solutions of 60 mg/L "free chlorine," 1200 mg/L "free chlorine," and nanopure water (control) at pH 7.0 and pH 8.5 for 24 hours. Thin sections were then analyzed to measure changes in the pyrite surfaces. For solution experiments, aquifer material was crushed to between 250 μm and 355 μm mesh sizes (S.A. ~ 50 cm^2/g – 60 cm^2/g, Foust et al. 1980) and reacted under the same conditions as the thin sections in a batch reactor. Solution samples were collected periodically during the 24 hour exposure and analyzed for arsenic, iron, and sulfate ion.

Pyrite oxidation is shown to dramatically increase with increasing chlorine concentrations as shown by measurements of released sulfate ion, used here as the reaction progress variable. EPMA maps also reveal complete oxidation of pyrite cements to Fe-oxyhydroxides at 1200 mg/L "free chlorine" and pH 7.0. This behavior does not occur at lower concentrations or higher pH. Arsenic release to solution does not appear to be directly correlated to increasing chlorine concentrations, but is governed by Fe-oxyhydroxide nucleation, which inhibits the release of dissolved arsenic at higher concentrations of chlorine.

ACKNOWLEDGEMENTS

First off I'd like acknowledge my funding sources. Initial funding for this project was provided by a seed grant from the Advance program at Virginia Tech. Additional funding was awarded from the Geological Society of America and the Wones Geologic Fund. The Wisconsin Department of Natural Resources granted money to our collaborators in Wisconsin, Madeline Gotkowitz, Eric Roden, and Evgenya Shelobolina.

I must thank my advisor Madeline Schreiber for admitting me to this great department, and allowing me to follow through on this project. She pushed me further than I thought I could go, and as a result I've learned not only about the field, but about how much I can take on and accomplish.

I also must acknowledge my former supervisors and colleagues at the USGS in Reston, VA for planting the graduate school seed. The work described in this paper could not have been completed without the generosity of Harvey Belkin at USGS Reston, for allowing me unlimited use of the Microbeam Lab. Jeff Kuhn in VT Dept. of Biology was also a great help for providing access to his ultracentrifuge. And thanks to Logan Park for rescuing my hard drive. The presence and encouragement of my wonderful friends made it fun to go through the graduate school process. Last I'd like to thank Nethers, for supporting me in my educational efforts.

TABLE OF CONTENTS

LIST OF FIGURES

1 INTRODUCTION

Arsenic (As) is a known carcinogen, linked to skin and internal cancers (NRC 1999). Due to health concerns, in 2006, the United States Environmental Protection Agency lowered the maximum contaminant level (MCL) of arsenic from 50 µg/L to 10 µg/L. Elevated concentrations of arsenic have been measured in groundwater across the United States, occurring in a wide variety of natural environments (Welch et al. 2000, Smedley and Kinniburgh 2002). One example is the Fox River Valley (FRV) of northeastern Wisconsin, in which elevated arsenic concentrations have been measured in groundwater within the St. Peter sandstone aquifer. In 2003, the Wisconsin Department of Natural Resources (WDNR) published a report estimating that 17% of domestic wells in the FRV contained arsenic concentrations exceeding 10 µg/L and approximately 4% of wells exceed 50 µg/L (Schreiber et al. 2003). Although the majority of wells in this region contain moderate arsenic concentrations (between 10 µg/L and 50 µg/L), individual wells have been reported to contain up to 12000 µg/L arsenic (Schreiber et al. 2003).

1.1 Arsenic and the St. Peter sandstone aquifer

The major aquifer in northeastern Wisconsin, the St. Peter sandstone, is comprised of Ordovician sandstone and is confined by the Ordovician Sinnipee dolomite. A deeper Cambrian sandstone aquifer occurs roughly 200 feet below the St. Peter sandstone, separated by the Prairie du Chein carbonate group. The youngest aquifer in

this system is an unconfined aquifer, which is made up of unconsolidated quaternary glacial deposits (Batten and Bradbury, 1996).

After deposition of the Ordovician sediments, Devonian aged brines moved through the system, precipitating a layer of sulfide minerals that is laterally extensive along the contact between the high conductivity St. Peter sandstone and the overlying Sinnipee dolomites (Girard and Barnes, 1995). This layer, referred to as the sulfide cement horizon (SCH) (Schreiber et al. 2000, Thornburg and Sahai 2004), contains continuous bands of sulfide cemented sandstones, as well as thick zones of sparsely occurring sulfide nodules (Schreiber et al. 2000). Previous investigations have identified these sulfides as predominantly pyrite and marcasite.

Bulk arsenic concentrations in sandstones hosting the SCH range from 20 mg/kg to 600 mg/kg (Gotkowitz et al. 2004) but arsenic measured in pyrite can reach weight percent values (Schreiber et al., 2000). Arsenic is thought to be incorporated in solid solution in pyrite grains with the high-arsenic zones occurring along euhedral pyrite grain boundaries. Although no discrete arsenic phases have been identified in the SCH (Schreiber et al. 2000, Thornburg and Sahai 2004, this study), iron oxides containing As have been identified.

Combined field and laboratory studies have demonstrated that in wells where the SCH is at the approximate elevation of the static water level in the borehole, As concentrations can greatly exceed 10 µg/L (Schreiber et al. 2000) due to oxidation of sulfides at the air-water-sulfide interface. Pumping tests on these arsenic-impacted wells show that after only a short period of pumping, As, Fe, and sulfate concentrations in well water rapidly decrease, suggesting that sulfide oxidation and subsequent As release

occurs in close proximity to the borehole as uncontaminated water quickly moves into the borehole during pumping (Schreiber et al. 2000, Gotkowitz et al. 2004).

When water levels are low, due to pumping or during periods of drought, the SCH may become exposed to air due to lowering water levels in the borehole. This is relevant because pyrite can be oxidized in humid environments, resulting in formation of weathering products such as jarosite and melanterite (Jerz and Rimstidt, 2004). These minerals can incorporate As and can be dissolved in groundwater as water levels rise during periods of non-pumping or under wetter conditions. As-bearing sulfate salts are not an important reservoir of As if the SCH remains under saturated conditions, but become relevant in boreholes that experience water level fluctuations due to pumping.

Another source of As to groundwater is iron oxyhydroxides, which are a weathering product of sulfide oxidation. Iron oxyhydroxides can strongly adsorb As (Stollenwerk 2003, Dixit and Hering 2003, Farquhar et al. 2002, Jain et al. 1999, Raven et al. 1998, Fendorf et al. 1997, Pierce an Moore, 1982), and thus can collect As from groundwater. There are several geochemical conditions which can promote release of As from the iron oxyhydroxide surface, such as desorption due to changes in pH or the presence of competitive oxyanions, such as phosphate (Stollenwerk, 2003, Pierce and Moore, 1982). Field studies have shown that borehole environments in the FRV can become highly reducing after only two days of non-pumping (Gotkowitz et al. 2004). Thus, reductive dissolution of the iron oxyhydroxides, a process which is microbially-mediated, can also be an important As-release mechanism in wells. Additionally, iron oxides that are rich in As can potentially be destabilized and deflocculate. Although iron oxyhydroxides have been generally observed to precipitate on quartz grains in sandstone

aquifers (Sasowsky et al. 2000), it is possible that pump action or other disturbances to the borehole could promote sloughing of freshly precipitated iron oxyhydroxides into well water.

1.2 Chlorine oxidation of pyrite

It is common practice for domestic well users to "shock treat" their wells with chlorine bleach to kill bacteria and remove biofilms that clog pipes and pumps. Because chlorine behaves as a strong oxidant, the WDNR currently recommends 10% the contact time and 20 % the concentration of chlorine shock treatments used in non As-impacted areas. This is due to the concern that the bleach will increase the rate and extent of pyrite oxidation, potentially exacerbating As contamination in the wells. A discussion of chlorine chemistry and chlorine oxidation of pyrite is thus relevant for this project.

Sodium hypochlorite (NaOCl) is the active ingredient in common household bleach. When mixed with water NaOCl rapidly dissociates to sodium, hydroxide, and hypochlorous acid (HOCl), following the reaction

$$NaOCl + H_2O \rightarrow Na^+ + HOCl + OH^- \quad (1)$$

Dissociation of hypochlorous acid to hypochlorite ion (OCl^-) has a pK_a of 7.5 and follows the reaction

$$HOCl \rightarrow OCl^- + H^+ \quad (2)$$

The oxidation of pyrite by dissolved oxygen in water is generally expressed as

$$2FeS_2 + 7O_2 + 2H_2O \rightarrow 2Fe^{2+} + 4SO_4^{2-} + 4H^+ \quad (3)$$

The oxidation reaction changes in the presence of bleach, where at pH above 7.5, hypochlorite is the dominant oxidant and oxidizes pyrite by the following reaction:

$2FeS_2 + 7OCl^- + H_2O \rightarrow Fe^{2+} + 2SO_4^{2-} + 7Cl^- + 2H^+$ (4)

At pH below 7.5, hypochlorous acid is the dominant oxidant and oxidizes pyrite by the following reaction:

$FeS_2 + 7HOCl + H_2O \rightarrow Fe^{2+} + 2SO_4^{2-} + 7Cl^- + 9H^+$ (5)

In this oxidizing environment, iron will rapidly oxidize and precipitate as iron oxides, following the reactions:

$Fe^{2+} + 0.5OCl^- + 2.5H_2O \rightarrow Fe(OH)_{3(s)} + 0.5Cl^- + 2H^+$ (6)

$Fe^{2+} + 0.5HOCl + 2.5H_2O \rightarrow Fe(OH)_{3(s)} + 0.5Cl^- + 2.5H^+$ (7)

This process occurs much more rapidly in the presence of chlorine species than by oxidation of iron by dissolved oxygen only (Lytle et al. 2004) and which follows the reaction:

$Fe^{2+} + ¼\ O_2 + 5/2\ H_2O \rightarrow Fe(OH)_3 + 2H^+$ (8)

Previous studies have shown that pH greatly affects the rate of pyrite oxidation by chlorine, with highest rates at low pH and decreasing at high pH (Umana and Leckie 1979). There are multiple pH dependent processes that control this behavior. The first pH-dependent process is the chlorine speciation dependence in aqueous solution. Between pH 2 and 7.5, hypochlorous acid is the predominant chlorine species. Above pH 7.5, hypochlorite ion is the dominant species. The second is the pH dependence of the surface charge of pyrite. At pH above 7, the surface charge of pyrite is negative. This negative surface charge could create an electrostatic repulsion between the pyrite surface and the negatively charged hypochlorite ion in solution. According to Umana and Leckie

(1979), this electrostatic effect would not occur at pH at or below 7, and there would be no repulsion between the pyrite surface and hypochlorous acid, a neutral chlorine species.

The hypothesis of this study is that the addition of chlorine bleach, which contains strong oxidants, to domestic wells open to As-bearing sulfides in the FRV increases the extent of pyrite oxidation, which can impact As release to drinking water. However, in the oxidizing conditions created by the chlorine species, the formation of Fe-oxides from sulfide oxidation can uptake the released As. A series of batch reactor and thin section experiments were designed to test this hypothesis and to provide data on oxidation of pyrite by chlorine that could be useful to the WDNR and other agencies managing As-impacted aquifer systems.

2 METHODS AND MATERIALS

Samples for the experiments were provided by Madeline Gotkowitz of the Wisconsin Geological and Natural History Survey. They were collected from Leonard Road Michaels Materials (LM) quarry in Winnebago County, Wisconsin. Parallel experiments were completed with thin sections and crushed LM material in order to evaluate the effects of variable chlorine concentrations on mineral surfaces and solution chemistry. Each sample (thin section or crushed solids) was exposed to a controlled chlorine solution for an experimental period of 24 hours. The three "free chlorine" concentrations ($[Cl_2] + [HOCl] + [OCl^-]$) chosen for these experiments were 0 mg/L (nanopure water control), 60 mg/L ("low dose" shock treatment), and 1200 mg/L ("high dose" shock treatment). The experiments were performed at pH 7.0 and pH 8.5 in an effort to distinguish differences in mineral surface chemistry and solution chemistry changes affected by each chlorine species. All experiments were performed in a Metrohm 719 S Titrino pH stat system. Solution pH was controlled using 0.1N NaOH. The solution was continuously stirred using a suspended propeller. The chlorine solutions were made by diluting newly opened bleach (Clorox) with nanopure water. The concentration of free chlorine was estimated using a colorimetric test (CHEMetrics Vacuettes kits K-2505C for high dose; CHEMetrics Vacuettes kits K-2505D for low dose).

2.1 Thin Section Experiments

Thin sections of LM quarry material were prepared to characterize the mineralogy and elemental composition of mineral surfaces before and after exposure to chlorine solutions. The thin sections were made by Spectrum Petrographics to a standard thickness of 30 microns with a single side microprobe polish. Each thin section was designated an experimental pH and "free chlorine" concentration prior to characterization, with two thin sections kept unexposed for use as controls. After treatment the thin sections were rinsed with nanopure water and dried in a vacuum oven. The thin sections were then held in an anaerobic chamber (Coy) until characterization to prevent further oxidation of the mineral surfaces.

Characterization of the thin sections was completed at the Microbeam Laboratory at the United States Geological Survey in Reston, VA. Thin sections were carbon coated prior to characterization. Quantitative analysis of sulfide minerals was run on the JEOL 8900 Electron Microprobe Analyzer (EPMA) at 20kV and 3x10-8 mA. Chemical standardization for quantitative analysis was completed to known standards. Element maps were run at 20kV and 5x10-8 mA at a 30msec dwell time.

2.2 Crushed material experiments

Crushed solids (250-355 micron) from the LM material were used in parallel experiments to increase reactive surface area for solution chemistry analysis. Bulk analysis of the crushed material shows an As concentration of 674 mg/kg. The crushed material was rinsed in nanopure water, dried in a vacuum oven, and then held in an

anaerobic chamber until use in experiments to prevent oxidation of the pyrite prior to exposure to chlorine solutions.

For each experiment, five grams of the solid material was reacted in 100 mL of solution (water, low dose chlorine, high dose chlorine) over a 24 hour period. Three 1 mL samples were collected at designated time steps. All sample aliquots were filtered (0.22 micron) to remove particles from solution. One unpreserved aliquot was used for SO_4^{2-} analysis to quantify the rate and extent of pyrite oxidation. Another was preserved with 0.1M HNO_3 to pH<2 after filtering and analyzed for Fe and As. The third was ultracentrifuged for 1 hour at 55,000 rpm to remove nanoparticles (Tadanier et al. 2005), and the supernatant was extracted and preserved with 0.1M HNO_3. Arsenic was analyzed using graphite furnace atomic absorption spectroscopy (GFAA; Varian Spectra220Z with Zeeman background correction). Iron was analyzed using the ferrozine method (Stookey, 1970) with absorbance read on a Beckman-Coulter DU 640 UV-Vis spectrophotometer at a fixed wavelength of 562 nm. Sulfate was analyzed by ion chromatography (Dionex DX-120). An additional experiment was performed on crushed LM material that had been washed a second time immediately before the experiment. The rinse was filtered (0.45 micron) and analyzed for As and SO_4^{2-}.

2.3 Analysis of Fe-oxides

Fe-oxides formed during the 1200 mg/L free chlorine experiment at pH 7.0 were collected from solution to determine amounts of adsorbed As. The Fe-oxides were allowed to settle onto a plastic tray in the reaction vessel, then centrifuged for 30 minutes at 13000 rpm. The Fe-oxide material was then transferred to a watch glass, rinsed with

nanopure water and dried in an oven. Five mg of the dried Fe-oxide material was digested for 72 hours in 1 ml 0.5 N HCl. The digestate was then analyzed for As.

3 RESULTS

3.1 Characterization of Pyrite Surfaces

EPMA and WDS analysis of pyrite surfaces prior to exposure to chlorine solutions reveal that As occurs in growth zones of euhedral grains at concentrations up to 0.9 weight percent. No independent As phase was detected. WDS analysis also reveals zones in pyrite that are enriched in other trace metals, including lead (Pb), copper (Cu), nickel (Ni), and cobalt (Co). Lead enrichment in pyrite reached 0.80 wt. %, while Ni, Cu, and Co reached 0.21 wt. %, 0.26 wt. %, and 0.11 wt. % respectively. Quantitative WDS and map analysis also reveal the occurrence of small grains of galena and chalcopyrite in the sulfide cement.

Figure 1 shows EPMA maps from section LM2-07-4. Pyrite grains forms cement between the large, dark, round quartz grains pictured in the top corners of images in Figure 1. Figure 1a shows a back scattered electron (BSE) image of the unreacted pyrite surface The BSE image shows that pyrite occurs as euhedral grains approximately 30μm to 100μm in diameter and as fine grained massive material. This massive material appears as zones of slightly lower iron (Fe) and sulfur (S) concentrations in the element maps (Figures 1c and 1d, respectively) because of limited element detection as a result of the rougher surfaces. The element map of As in the unreacted pyrite surface shows zoning in the euhedral grains, as seen in Figure 1b.

Figure 2 shows EPMA maps of section LM2-07-5 after 24 hour exposure to the control solution (nanopure water) at pH 7.0. Figure 2a reveals the presence of small (~10 μm) secondary minerals forming on the rough-textured, fine-grained surfaces. Figure 2d

shows that these grains contain Fe but not S, suggesting that they are small clusters of Fe-oxides. The fine-grained pyrite textures on which these oxides grow provide a maximum surface area for pyrite oxidation and subsequent Fe-oxide precipitation. Figure 2b reveals that As remains zoned in the euhedral pyrite grains after 24 hour exposure to nanopure water at pH 7.0.

EPMA maps of section LM2-07-3 after 24 hour exposure to the low dose chlorine treatment at pH 7.0 are pictured in Figure 3. Figure 3a (BSE) shows large (~ 100 μm) clusters of Fe-oxides on the pitted pyrite surface. In some areas the pyrite has been completely dissolved and cracks occur across the thin section. These Fe-oxides are easily recognizable in the Fe and S maps (Figures 3c and 3d, respectively) as the relatively large areas (100 μm – 200 μm across) simultaneously enriched in Fe and depleted in S. After 24 hour exposure to the low dose solution at pH 7.0, As rich zones remain in the euhedral pyrite grains.

Complete oxidation of the pyrite cements to Fe-oxides is shown in Figure 4. These EPMA images are of section LM2-07-2 after 24 hour exposure to the high dose solution at pH 7.0. The BSE image (Figure 4a) shows a desiccated surface of large Fe-oxides, replacing what was previously pyrite, surrounding quartz grains. Figure 4d shows that almost no S remains in the mineral. Iron concentrations remain high (Figure 4c), but As zoning is no longer visible.

Figure 5 shows section LM1-07-1 after 24 hour exposure to nanopure water at pH 8.5. The BSE image (Figure 5a) shows euhedral pyrite grains occurring with fine grained massive pyrite. The individual euhedral grains range in size from approximately 10 μm to 80 μm in diameter. Unlike the sample exposed to nanopure water held at pH 7.0, at pH

8.5 there is no occurrence of small Fe-oxides on the rough, fine-grained surfaces. Zones of As are not visible in the euhedral grains in section LM1-07-1, but rather occur in small regions near contact with quartz grains. This is not an artifact of the exposure solution, but simply a result of sample cutting and imaging location on the sample.

After 24 hour exposure to the low dose chlorine treatment at pH 8.5, section LM1-07-4 does not exhibit extensive formation of Fe-oxides forming on the pyrite surfaces (Figure 6a). However, close inspection of Figure 6c reveals a few very small (< 10 μm) clusters of Fe-enriched minerals. These areas of Fe enrichment correspond to S depletion (Figure 6d). Larger zones (100 μm – 200 μm across) of moderate S depletion occur on the surface of section LM1-07-4. Although these zones do not correspond to areas of Fe-enrichment, so Fe-oxide formation has likely not yet occurred in these areas, but the S depletion does suggest the removal of S from the pyrite. Arsenic in section LM1-07-4 occurs as pockets of enrichment in the pyrite cement (Figure 6b), but is not shown as distinct zones in the pyrite crystals.

Figure 7 shows section LM1-07-2 after 24 hour exposure to 1200 mg/L chlorine at pH 8.5. Iron oxides are shown to occur as layers, peeling back from the pyrite surface (Figure 7a). Zones of Fe enrichment corresponding with zones of S depletion shown in Figures 7c and 7d suggest that this material is an Fe-oxide mineral. Most of the pyrite remains intact, which was not the case for the high dose chlorine treatment at pH 7.0. Arsenic is visible in zones in a euhedral pyrite grain, and also as areas of enrichment near contacts with quartz grains.

3.2 Batch reactor experiments

Results of batch reactions are presented in Figures 8 through 10. Figure 8a shows sulfate release during 24 hour exposure of crushed LM material to water, 60 mg/L free chlorine, and 1200 mg/L free chlorine, as well as the double washed experiment at pH 7.0. Sulfate levels increase rapidly after initial contact between LM material and solution, reaching near maximum levels within 3 hours for all three solutions. At 24 hours, the greatest concentrations of sulfate (914 mg/L) were measured in the 1200 mg/L free chlorine experiment, with lower concentrations measured in the 60 mg/L chlorine solution (632 mg/L) and in water (587 mg/L single-washed, 365 mg/L double-washed).

Sulfate release to solution was lower at pH 8.5 than at pH 7.0. Figure 8b shows that sulfate release is still highest during exposure to 1200 mg/L free chlorine, reaching 777 mg/L after 24 hours. Maximum sulfate concentrations released in 60 mg/L free chlorine and water were 495 mg/L and 467 mg/L, respectively, after 24 hours. The patterns of sulfate at pH 8.5 are similar to those seen at pH 7.0, with concentrations increasing rapidly until approximately 3 hours and reaching near maximum levels after 8 hours.

Although both filtered (0.22 μm) and ultracentrifuged samples were analyzed for As, the concentrations were almost identical, indicating that all As released to solution was dissolved and not associated with particles. In general, As release to solution does not mimic sulfate release (Figure 9). The exceptions are the pH 7.0 water experiments (Figure 9a), which demonstrate rapid increase in As concentrations within the first 3 hours, reaching near maximum concentrations (mean 21 μg/L, range 16-26 μg/L for single rinsed solids, 20 μg/L for double washed) at 8 hours. Patterns of arsenic release

are different in chlorine solutions at pH 7.0. In the 60 mg/L free chorine experiment, As concentrations are below detection until 8 hours, at which point concentrations increase steadily to 6 µg/L by 24 hours. In the 1200 mg/L free chlorine experiment, As concentrations spike at 15 minutes (7 µg/L), then decrease to < 2 µg/L until 8 hours, after which they slowly increase to approximately 6 µg/L by 24 hours.

Figure 9b shows As release to solution at pH 8.5. In the water experiment, after an initial spike at the first sampling (0 minutes) of As (4 µg/L), concentrations of As in solution increase steadily to 12 µg/L at 24 hours, a similar pattern as that observed in the pH 7.0 water experiment. Arsenic concentrations in the 60 mg/L free chlorine experiment also spiked (3 µg/L) in the first hour, but subsequent sampling shows steady increases of As to a maximum of 7 µg/L at 24 hours. In the 1200 mg/L free chlorine experiment, As concentrations spiked twice in the first 15 minutes, then gradually increased over time reaching 18 µg/L at 24 hours.

Iron (0.22 µm filtered) release to solution at pH 7.0 and 8.5 is shown in Figures 10a and 10b, respectively. Dissolved (i.e., ultracentrifuged) Fe data are not shown as with only a few exceptions, concentrations were very close to the detection limit, indicating that most of the Fe released to solution was associated with small particles (<0.22 µm). Similar to As, Fe concentrations measured in solution are highest in the pH 7.0 water experiment (Figure 10a, only total Fe shown). In the 60 m/L free chlorine experiment, Fe spiked (10 µg/L) within the first 10 minutes, but decreased to < 5 µg/L for the remainder of the experiment. In 1200 mg/L free chlorine experiment, Fe concentrations were below detection until 60 minutes, after which total Fe concentrations steadily increased to a maximum of 120 µg/L at 24 hours.

Figures 10b shows Fe concentrations in the pH 8.5 experiments. In the water experiment, Fe concentrations spiked (815 µg/L) at 5 minutes, but were low (<50 µg/L) for the remainder of the experiment. In the 60 mg/L free chlorine experiment, Fe concentrations are less than 50 µg/L with the exception of one spike (250 µg/L) at 15 minutes. In the 1200 mg/L free chlorine experiment, Fe concentrations fluctuate over the course of the experiment, reaching a maximum of approximately 450 µg/L at 24 hours.

Post-experimental digestion and analysis of iron oxides collected from the pH 7 1200 mg/L experiment reveals an arsenic concentration of 2460 mg/kg.

4 DISCUSSION

4.1 Reservoirs of arsenic

Results of the electron microprobe analysis show that arsenic occurs in the LM thin sections in association with pyrite, and appears to be adsorbed onto Fe-oxide surfaces, as has been reported in other studies on the sulfide cement horizon (e.g. Schreiber et al. 2000). Although Fe-oxides were not observed on the pre-reacted thin sections from the LM material, they were observed in SCH samples collected from other localities within the Fox River Valley. EPMA analyses revealed distinct zones of As enrichment in euhedral pyrite grains in the LM sections at concentrations up to 1 wt. %. Elevated As concentrations were not noticed in the smaller massive pyrite grains.

EPMA analysis did not reveal discrete As phases. However, analysis of rinse water from the pre-experimental wash of the crushed LM material showed elevated concentrations of dissolved As (18 μg/L) and SO_4^{2-} (197 mg/L), suggesting the presence of As-bearing soluble salts. As reported by Jerz and Rimstidt (2004), jarosite and melanterite will form as oxidation products of pyrite in humid air and can incorporate As. Due to their high solubility, the As-bearing salts would not likely form in the saturated zone, but could act as an additional As host in boreholes where static water levels in wells fluctuate, allowing for exposure and oxidation of pyrite in the SCH by oxygen and water in humid air. Pumping practices would greatly impact the formation of these salts, as well as their subsequent dissolution and contribution of As to groundwater.

4.2 Role of chlorine in pyrite oxidation

Results from both the thin section and batch reaction experiments suggest that introducing chlorine to this system enhances pyrite oxidation. The relative oxidizing power of the high dose solution (1.69×10^{-2} mol/L Cl_2) is approximately 100 times greater than that of dissolved oxygen in air-saturated water (DO of 8 mg/L = 2.5×10^{-4} mol/L O_2), while the relative oxidizing power of the low dose solution (8.45×10^{-4} mol/L Cl_2) is approximately four times greater than that of air-saturated water. Solution pH also plays a role in pyrite oxidation, with higher sulfate release, and hence higher rates of sulfide oxidation, at the lower pH. This pH effect is related to the chlorine speciation differences with changing pH, where at pH 7.0 approximately 80% of chlorine is in the HOCl state, and at pH 8.5 approximately 90% of chlorine is in the OCl- state (Umana and Leckie, 1979). Umana and Leckie also reported similar trends of higher oxidation rates of pyrite by chlorine at lower pH.

4.3 Role of chlorine in iron oxide formation

During the experiments, it was observed that formation of iron oxide was most significant in the high dose chlorine solutions. During pyrite oxidation, Fe is released from pyrite as ferrous iron (Equations 4 and 5); which will subsequently oxidize and precipitate as Fe(III) oxides (Equations 6 and 7). As mentioned above, the chlorine solutions have approximately four to one hundred times greater the oxidizing power than air saturated water based on molar quantities of the oxidants in solution. In addition to impacting pyrite oxidation, the higher oxidizing strength of chlorine solutions will

increase the rate of oxidation of ferrous iron, thus promoting faster and more extensive Fe-oxide precipitation.

Previous studies on chlorine promoted oxidation of ferrous iron have suggested that the rate of oxidation of ferrous iron controls the physical and chemical properties of the nucleating oxyhydroxides (Lytle et al. 2004). In pure water, Fe-oxide precipitation is slow, allowing dissolved iron to oxidize both in solution and on the surfaces of nucleating Fe-oxides, which can form dense aggregates of Fe-oxides over time (Lytle et al. 2004). In systems with highly oxidizing conditions created by chlorine addition, Fe-oxides precipitate rapidly and cannot form the dense aggregates that are observed to form in pure water. Another feature of the loose Fe-oxide aggregates formed by rapid ferrous iron oxidation is a higher surface area than those precipitated in pure water (Lytle et al. 2004). The rapid nucleation rate and physical properties of Fe-oxides formed in chlorine solutions will exert control on As released from pyrite oxidation due to the affinity of As to sorb to Fe-oxide surfaces.

4.4 Role of chlorine in As cycling

Results of these experiments suggest that arsenic mobility is controlled by a combination of pyrite oxidation and Fe-oxide precipitation. Pyrite oxidation increases with increasing chlorine concentrations and decreases slightly with increasing pH. Fe-oxide precipitation as a result of ferrous iron oxidation is also positively correlated with increasing chlorine concentrations and negatively correlated with increasing pH as observed in EPMA maps.

A visual summary of As release pathways as a result of oxidation is shown in Figure 11. Pyrite oxidation is the first mobilization pathway for As. Oxidation is greatest with the addition of chlorine, followed by oxidation by oxygen in air and then oxidation by dissolved oxygen in water (Jerz and Rimstidt, 2004). The reactions for these pathways are numbered and correspond to reactions discussed in the introduction. The result of pyrite oxidation by all three oxidants is the release of sulfate, ferrous iron, and As to solution. Subsequent oxidation of ferrous iron by either chlorine or DO results in the precipitation of Fe-oxides. Arsenic released to solution may then adsorbed by the Fe-oxides and at least partially removed from solution. The results of these experiments then imply that with increasing chlorine concentrations, there is greater oxidation of pyrite, releasing more As, but there is also greater release and oxidation of ferrous iron, resulting in greater sorption capacity of Fe-oxides to remove As from solution. According to the measured amounts of sulfate released, and the stoichiometry in Equations 3 and 4, if the pyrite in the LM material contains on average 0.1 weight percent As, there should be approximately 1000 µg/L As being released to solution during the high dose experiments. However, the highest levels measured in solution are only two percent of this value. This is due adsorption of As by Fe-oxides. Digestion and analysis of Fe-oxides from the pH 7.0 high dose experiment revealed As concentrations of 2460 mg/kg, indicating that much of the As released from pyrite oxidation was removed by the formation of Fe-oxides.

The highest levels of As were released during the high dose experiment at pH 8.5. There was more than twice the amount of As measured in the low dose experiment at pH 8.5 and more than 3 times greater than that measured in the high dose experiment at pH

7.0. Analyses of ultracentrifuged samples showed essentially the same concentrations of As as the filtered samples, indicating that the As measured solution was not associated with particles. A possible explanation for the high As concentrations at pH 8.5 is the pH dependence of Fe-oxide sorption capability. The sorption mechanism of arsenate on Fe-oxide is impeded at above neutral pH due to a quasi-negative surface charge created by hydroxyl association with the Fe-oxide surface (Dzombak and Morel, 1990). The point of zero charge (PZC) for ferrihydrite is 8.0, and goethite is 7.7. Electrostatic repulsion at the higher pH inhibits the ability of the negatively charged arsenate molecule to complex with the Fe-oxide surface, leading to lower adsorption and hence, higher As concentrations in solution. The PZC values for both Fe-oxides are below pH 8.5, suggesting that the higher As concentrations measured at pH 8.5 could be due to the desorption of As from the Fe-oxide surfaces.

4.5 Implications

Chlorine promoted oxidation affects As mobility in the St. Peter Aquifer in two ways. Introduction of chlorine to solution increases dissolution of pyrite in SCH, releasing more As from the pyrite structure, and also increases the rate of Fe-oxide precipitation and subsequent uptake of As in solution. The effect of chlorine on Fe-oxide precipitation is also two fold: 1) chlorine promotes increased oxidation of pyrite (observed for the high dose only), releasing more dissolved ferrous iron, and 2) chlorine increases oxidation of the released ferrous iron to Fe-oxides. Arsenic uptake by Fe-oxides is substantial but is slightly affected by solution pH, where higher pH causes a lowered capacity of Fe-oxides to adsorb arsenate, resulting in higher As concentrations in

solution. This pH dependence is a concern in the St. Peter aquifer, where the overlying Sinnipee carbonate group buffers the pH of groundwater.

Results of this study suggest that decreasing chlorine concentrations in well disinfection treatments will not decrease As release to drinking water, but may in fact promote As release due to decreased amounts of Fe-oxide nucleation. However, it is important to consider that arsenic adsorbed to Fe-oxide surfaces may be made available for re-release if conditions in the borehole become reducing, which happens rapidly after periods of non-pumping as suggested by field studies conducted by Gotkowitz et al. (2004). Arsenic can also be mobilized in drinking water if deflocculation of As-bearing Fe-oxides occurs, forming highly mobile colloids and nanoparticles (Tadanier et al. 2005). Arsenic release from reductive dissolution of Fe-oxides, or transport on Fe-oxide particles could be a secondary release mechanism that would be indirectly affected by an increase in pyrite oxidation promoted by chlorine disinfection.

Results from this research also have implications for water quality issues related to aquifer storage and recovery (ASR). During this procedure, treated surface water is pumped into confined aquifers that may be recovered during times of drought. In many cases these aquifers have not been previously exposed to oxidizing conditions, which can cause the release of contaminants to the stored water. Municipalities in south western Florida are experiencing elevated As concentrations in groundwater after ASR procedures, where before As was at background levels. (Price and Pichler, 2006; Jones and Pichler, 2007).

Treated waste water often contains residual chlorine as well as dissolved oxygen. For instance, water used for ASR injection in Tampa, FL contains approximately 30

mg/L chlorine and 15 mg/L DO (Jones and Pichler, 2007). Results reported in this paper, as well as those cited (Price and Pichler, 2006; Jones and Pichler, 2007) indicate that introducing aquifer solids that contain As-bearing pyrite to these oxidants could initiate the oxidation of pyrite and release of As. Fe-oxide formation has not been reported in studies of ASR in Florida, although they may act as a sink for As in these systems. Microbially-mediated reduction of Fe-oxides could produce a secondary pathway for As release in southern Florida, and pH could play a role in As sorption. The aquifers used in ASR procedures in southern Florida are limestone aquifers, and pH of groundwater in the area ranges from 6.9 to 8.7 (Jones and Pichler, 2007).

Another factor that has potential to impact As mobility in ASR systems is the presence of nutrients in injected water. Denitrification has been linked to pyrite oxidation in systems where oxygen has been consumed (Postma et al. 1991). If nitrate is present in treated wastewater used in ASR injection, this could provide another oxidant to the aquifer system. Phosphate, another common nutrient, competes with As on Fe-oxide sorption sites (Smedley and Kinniburgh 2002, Pierce and Moore 1982), which could cause release of As to groundwater in areas where phosphate rich water is injected. Applying results found in this study could be useful in further understanding the mechanisms for As release and mobility in ASR systems.

REFERENCES

[1-25]

1. Batten, W. and K. Bradbury, *Regional groundwater flow system between Wolf and Fox Rivers near Green Bay, Wisconsin.* Information Circular 75. Wisconsin Geologic and Natural History Survey, Madison Wisconsin, 1996.
2. Dixit, S. and J.G. Hering, *Comparison of arsenic(V) and arsenic(III) sorption onto iron oxide minerals: Implications for arsenic mobility.* Environmental Science & Technology, 2003. **37**(18): p. 4182-4189.
3. Dzombak, D.A. and F.M.M. Morel, *Surface Complexation Modeling: Hydrous Ferric Oxide*. 1990. 393.
4. Farquhar, M.L., et al., *Mechanisms of arsenic uptake from aqueous solution by interaction with goethite, lepidocrocite, mackinawite, and pyrite: An X-ray absorption spectroscopy study*. Environmental Science & Technology, 2002. **36**(8): p. 1757-1762.
5. Fendorf, S., et al., *Arsenate and chromate retention mechanisms on goethite .1. Surface structure.* Environmental Science & Technology, 1997. **31**(2): p. 315-320.
6. Foust, A.S., et al., *Principles of Unit Operations*. 1980, New York: John Wiley and Sons.
7. Girard, J. and D. Barnes, *Illitization and paleothermal regimes in the Middle Ordovician St. Peter Sandstone, central Michigan Basin: K-Ar, oxigen isotope, and fluid inclusion data.* AAPG Bull 79, 1995: p. 49-69.
8. Gotkowitz, M.B., M.E. Schreiber, and J.A. Sim, *Effects of water use on arsenic release to well water in a confined aquifer.* Ground Water, 2004. **42**(4): p. 568-575.
9. Jain, A., K.P. Raven, and R.H. Loeppert, *Arsenite and arsenate adsorption on ferrihydrite: Surface charge reduction and net OH- release stoichiometry.* Environmental Science & Technology, 1999. **33**(8): p. 1179-1184.
10. Jerz, J.K. and J.D. Rimstidt, *Pyrite oxidation in moist air.* Geochimica Et Cosmochimica Acta, 2004. **68**(4): p. 701-714.
11. Jones, G.W. and T. Pichler, *Relationship between pyrite stability and arsenic mobility during aquifer storage and recovery in southwest central Florida.* Environmental Science & Technology, 2007. **41**(3): p. 723-730.
12. Lytle, D.A., M.L. Magnuson, and V.L. Snoeyink, *Effect of oxidants on the properties of Fe(III) particles and suspensions formed from the oxidation of Fe(II).* Journal American Water Works Association, 2004. **96**(8): p. 112-124.
13. NRC, ed. *Arsenic in Drinking Water*. 1999, National Academy Press: Washington, DC.
14. Pierce, M.L. and C.B. Moore, *Adsorption of Arsenite and Arsenate on Amorphous Iron Hydroxide.* Water Research, 1982. **16**(7): p. 1247-1253.
15. Postma, D., et al., *Nitrate Reduction in an Unconfined Sandy Aquifer - Water Chemistry, Reduction Processes, and Geochemical Modeling.* Water Resources Research, 1991. **27**(8): p. 2027-2045.

16. Price, R.E. and T. Pichler, *Abundance and mineralogical association of arsenic in the Suwannee Limestone (Florida): Implications for arsenic release during water-rock interaction.* Chemical Geology, 2006. **228**(1-3): p. 44-56.
17. Raven, K.P., A. Jain, and R.H. Loeppert, *Arsenite and arsenate adsorption on ferrihydrite: Kinetics, equilibrium, and adsorption envelopes.* Environmental Science & Technology, 1998. **32**(3): p. 344-349.
18. Sasowsky, I.D., A. Foos, and C.M. Miller, *Lithic controls on the removal of iron and remediation of acidic mine drainage.* Water Research, 2000. **34**(10): p. 2742-2746.
19. Schreiber, M.E., et al., *Mechanisms of arsenic release to groundwater from naturally occurring sources, Eastern Wisconsin,* in *Arsenic in Groundwater,* A.H. Welch and K. Stollenwerk, Editors. 2003, Kluwer Publishers. p. 259-280.
20. Schreiber, M.E., J.A. Simo, and P.G. Freiberg, *Stratigraphic and geochemical controls on naturally occurring arsenic in groundwater, eastern Wisconsin, USA.* Hydrogeology Journal, 2000. **8**(2): p. 161-176.
21. Smedley, P.L. and D.G. Kinniburgh, *A review of the source, behaviour and distribution of arsenic in natural waters.* Applied Geochemistry, 2002. **17**(5): p. 517-568.
22. Tadanier, C.J., M.E. Schreiber, and J.W. Roller, *Arsenic mobilization through microbially mediated deflocculation of ferrihydrite.* Environmental Science & Technology, 2005. **39**(9): p. 3061-3068.
23. Thornburg, K. and N. Sahai, *Arsenic occurrence, mobility, and 14 retardation in sandstone and dolomite formations of the Fox River Valley, eastern Wisconsin.* Environmental Science & Technology, 2004. **38**(19): p. 5087-5094.
24. Umana, A.F. and J.O. Leckie, *Kinetics of Oxidative Dissolution of Pyrite by Aqueous Chlorine Species.* Abstracts of Papers of the American Chemical Society, 1978. **176**(Sep): p. 170-170.
25. Welch, A.H., et al., *Arsenic in ground water of the United States: Occurrence and geochemistry.* Ground Water, 2000. **38**(4): p. 589-604.

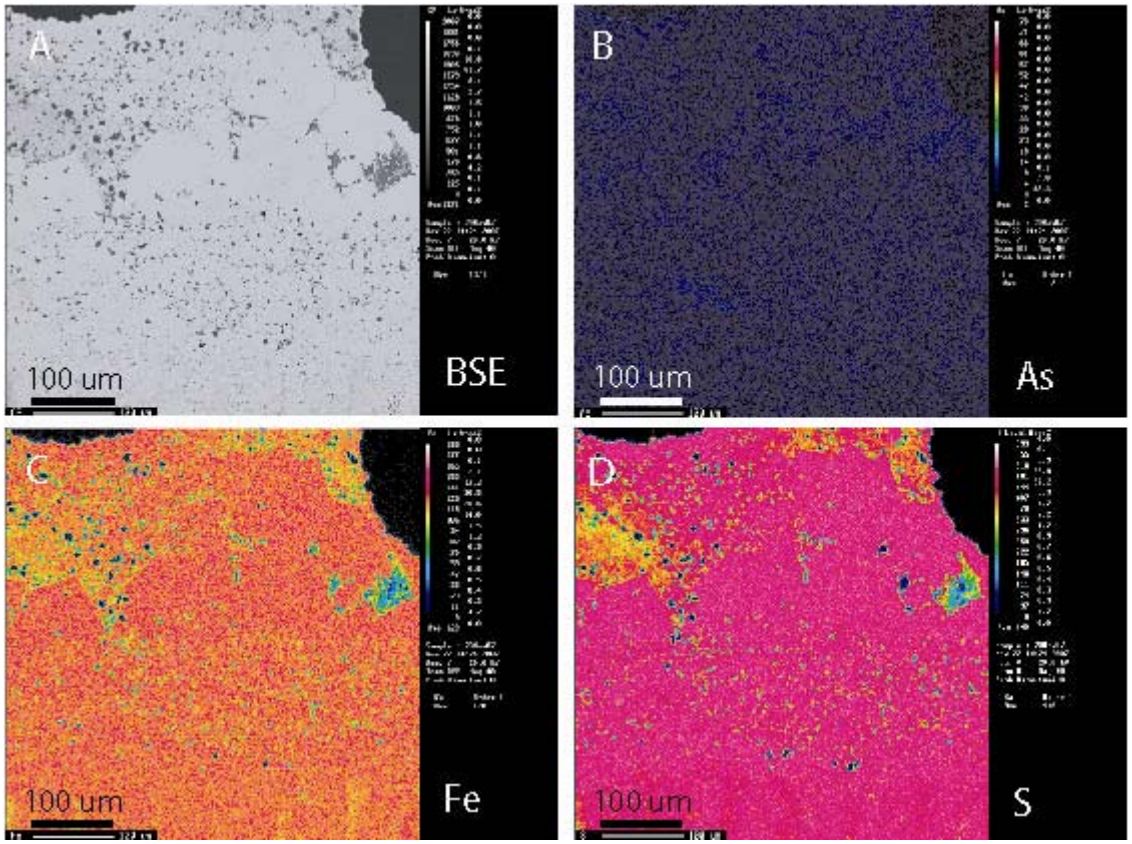

Figure 1 0.5 mm x 0.5 mm EPMA element maps of thin section LM2-07-4. Thin section was not exposed to solution prior to analysis. Concentrations indicated on color bars on the right side of each image. Warm colors indicate zones of high concentrations, cool colors indicate zones of low concentrations. A) Back scattered electron image B) As C) Fe D) S Euhedral pyrite occurs with massive pyrite as cement between quartz grains seen in these images as large, rounded dark areas.

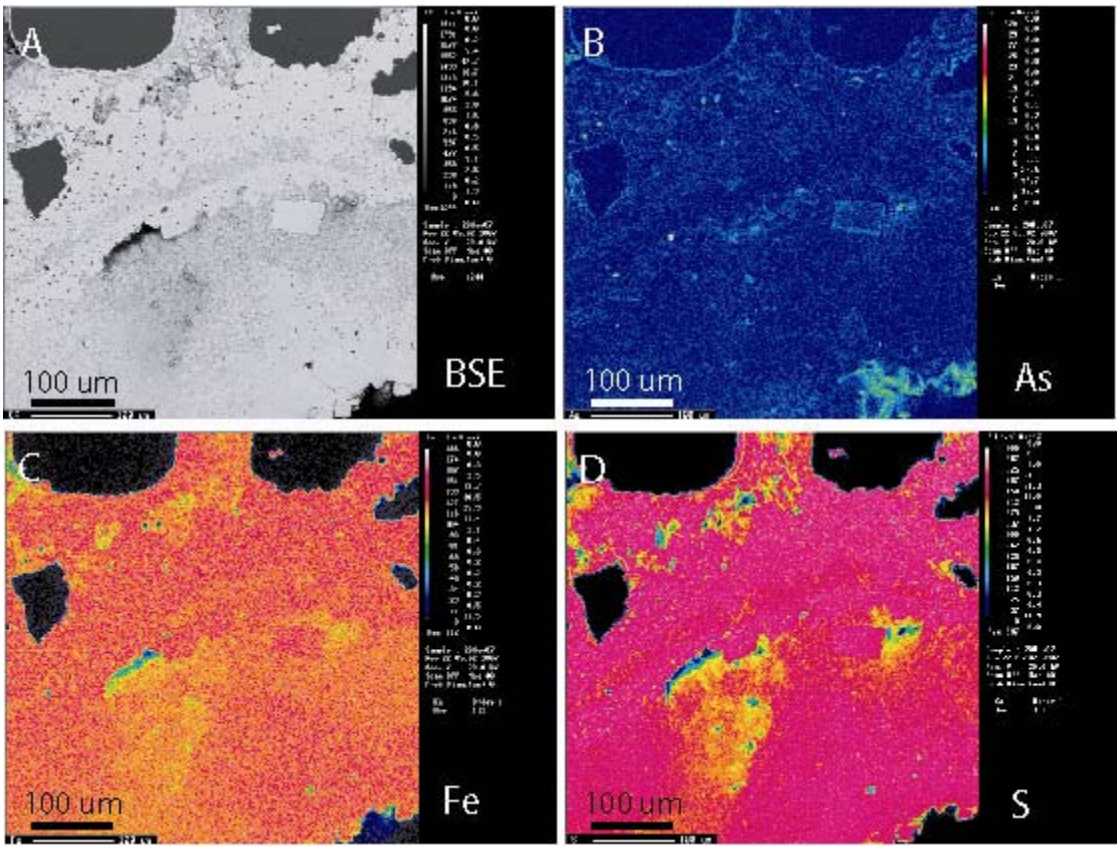

Figure 2 0.5 mm x 0.5 mm EPMA element maps of thin section LM2-07-5 after 24 hour exposure to nanopure water at pH 7.0. Concentrations indicated on color bars on the right side of each image. Warm colors indicate zones of high concentrations, cool colors indicate zones of low concentrations. A) Back scattered electron image B) As C) Fe D) S Small secondary minerals occur on massive pyrite visible as areas depleted in S and enriched in Fe. Zones enriched in As are visible in grain boundaries of euhedral pyrite.

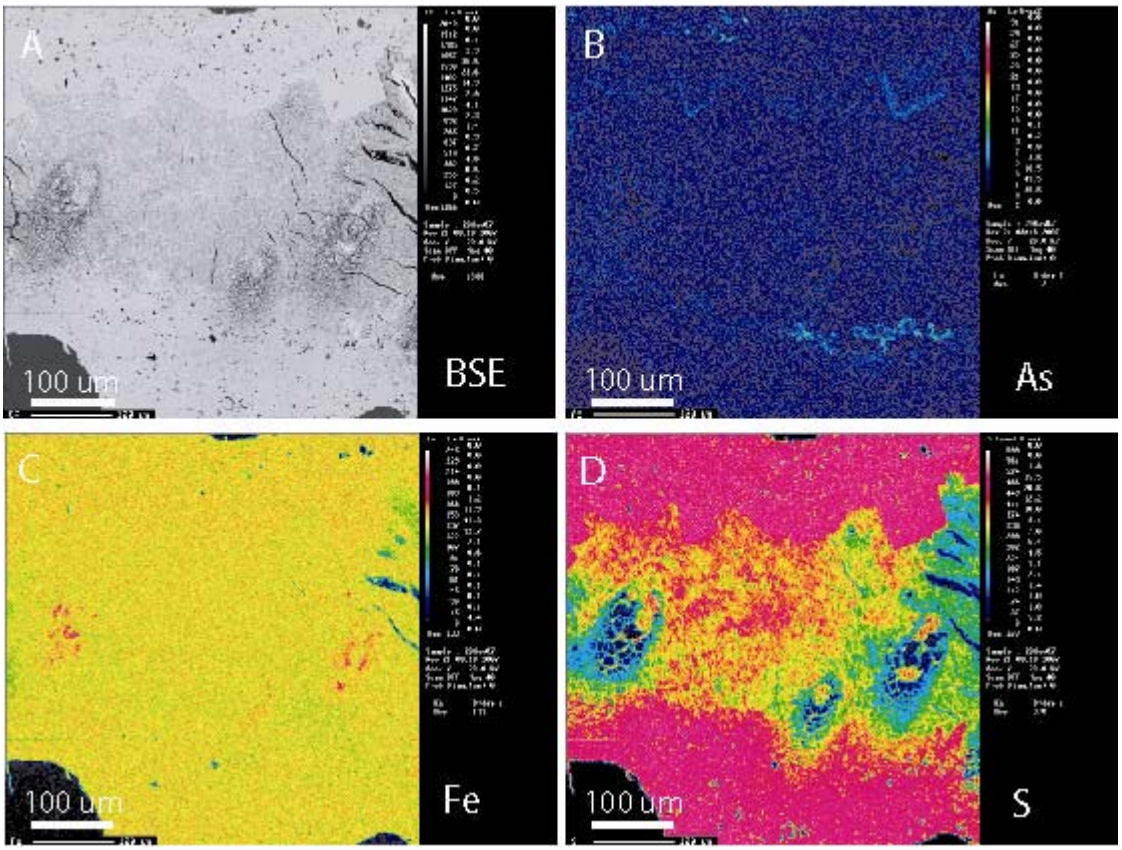

Figure 3 0.5 mm x 0.5 mm EPMA element maps of thin section LM2-07-3 after 24 hour exposure to 60 mg/L free chlorine at pH 7.0. Concentrations indicated on color bars on the right side of each image. Warm colors indicate zones of high concentrations, cool colors indicate zones of low concentrations. A) Back scattered electron image B) As C) Fe D) S Large Fe-oxides (~ 100 microns in diameter) occur on pitted pyrite visible as areas enriched in Fe and depleted in S. Zones enriched in As are still visible in grain boundaries of euhedral pyrite.

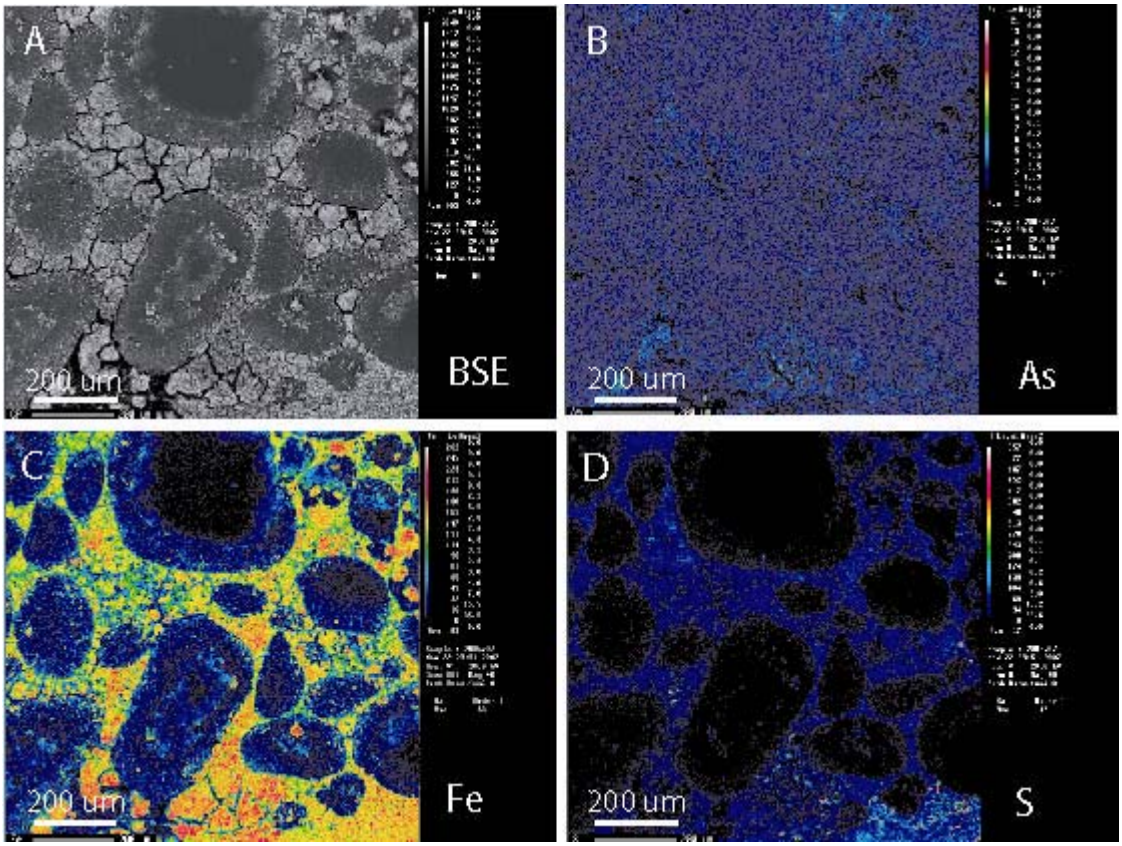

Figure 4 1 mm x 1 mm EPMA element maps of thin section LM2-07-2 after 24 hour exposure to 1200 mg/L free chlorine at pH 7.0. Concentrations indicated on color bars on the right side of each image. Warm colors indicate zones of high concentrations, cool colors indicate zones of low concentrations. A) Back scattered electron image B) As C) Fe D) S Pyrite cements have been completely oxidized and replaced by Fe-oxides. Fe-oxides appear as crusts between rounded quartz grains. No S remains on the surface, though elevated Fe concentrations are still visible. Arsenic zoning is no longer visible as no euhedral pyrite remains.

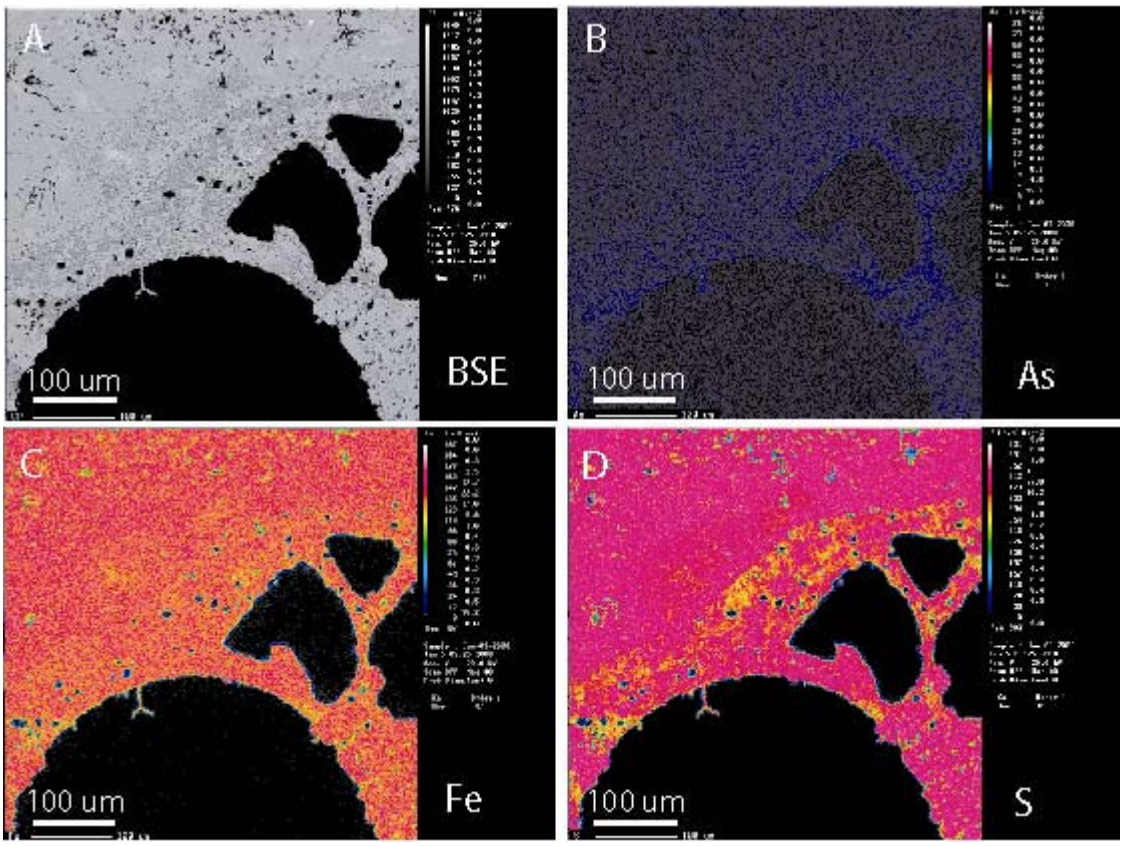

Figure 5 0.5 mm x 0.5 mm EPMA element maps of thin section LM1-07-1 after 24 hour exposure to nanopure water at pH 8.5. Concentrations indicated on color bars on the right side of each image. Warm colors indicate zones of high concentrations, cool colors indicate zones of low concentrations. A) Back scattered electron image B) As C) Fe D) S No visible evidence of pyrite oxidation or Fe-oxide nucleation occurs after exposure.

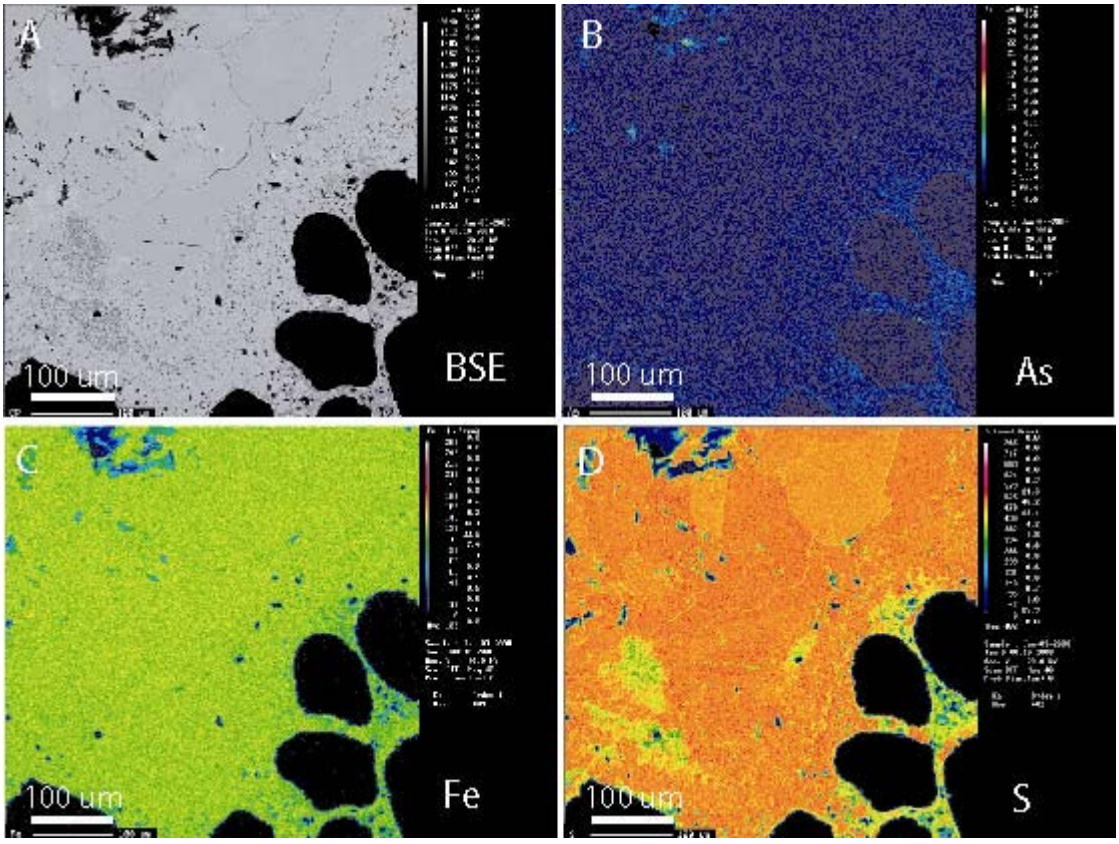

Figure 6 0.5 mm x 0.5 mm EPMA element maps of thin section LM1-07-4 after 24 hour exposure to 60 mg/L free chlorine at pH 8.5. Concentrations indicated on color bars on the right side of each image. Warm colors indicate zones of high concentrations, cool colors indicate zones of low concentrations. A) Back scattered electron image B) As C) Fe D) S Very small Fe-oxides (< 10 microns in diameter) occur on pyrite surfaces visible as areas enriched in Fe and depleted in S in the NW quadrant of the images. Broad zones of S depletion also occur on pyrite surfaces but are not accompanied by Fe-enrichment.

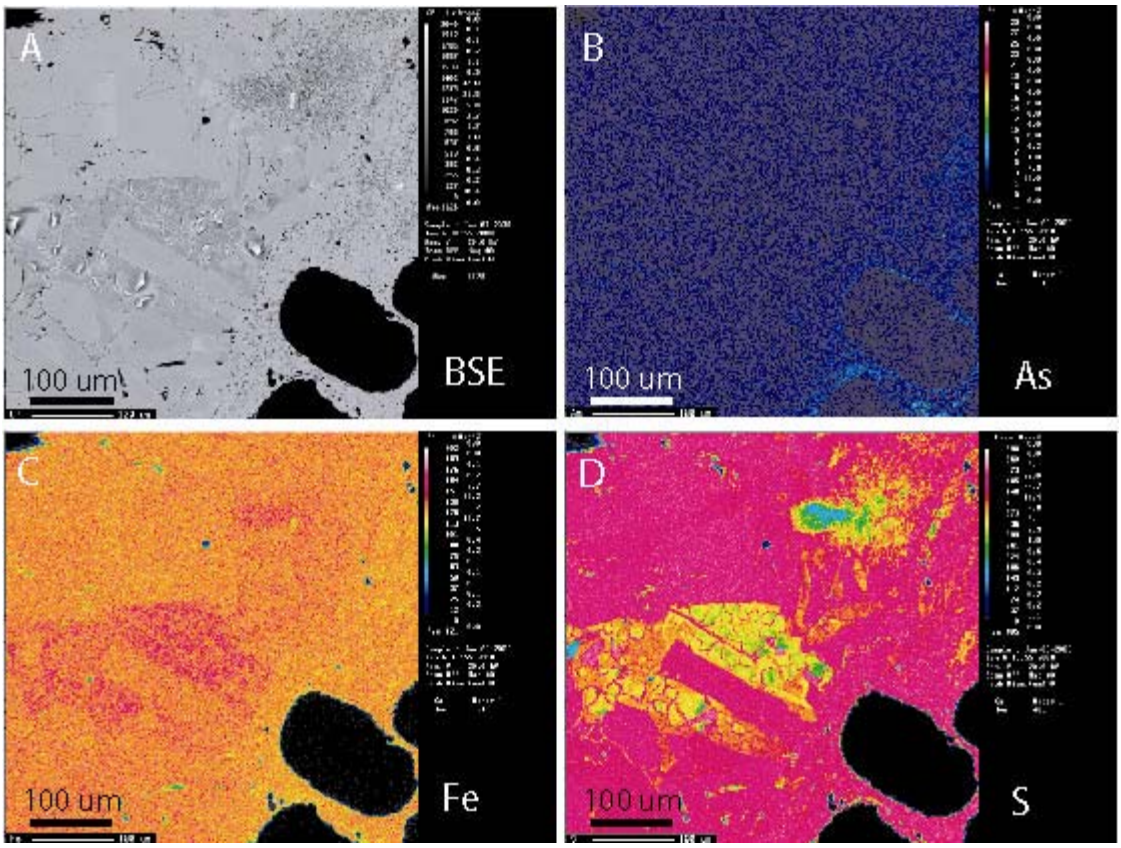

Figure 7 0.5 mm x 0.5 mm EPMA element maps of thin section LM1-07-2 after 24 hour exposure to 1200 mg/L free chlorine at pH 8.5. Concentrations indicated on color bars on the right side of each image. Warm colors indicate zones of high concentrations, cool colors indicate zones of low concentrations. A) Back scattered electron image B) As C) Fe D) S Fe-oxides occur as thin sheets after exposure and appear to peel back from the pyrite surface. Note that complete replacement of pyrite by Fe-oxides does not occur after exposure to high dose solution at pH 8.5 as it did at pH 7.0.

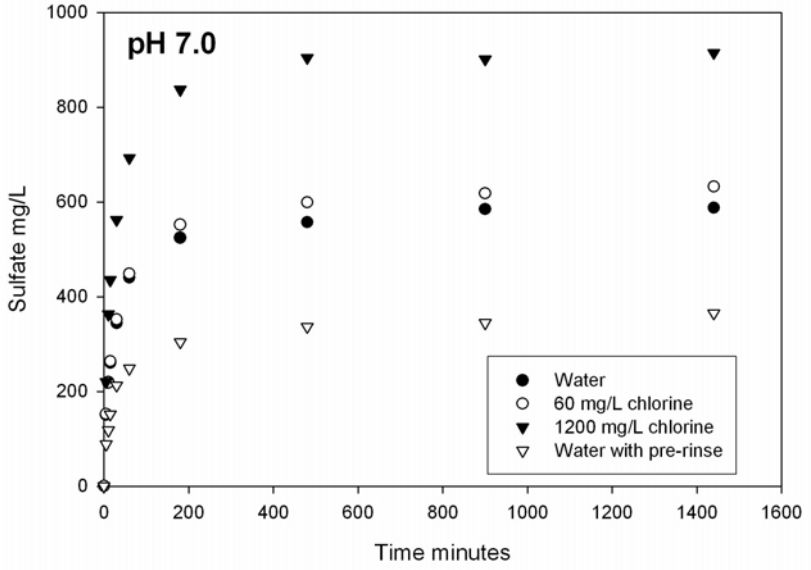

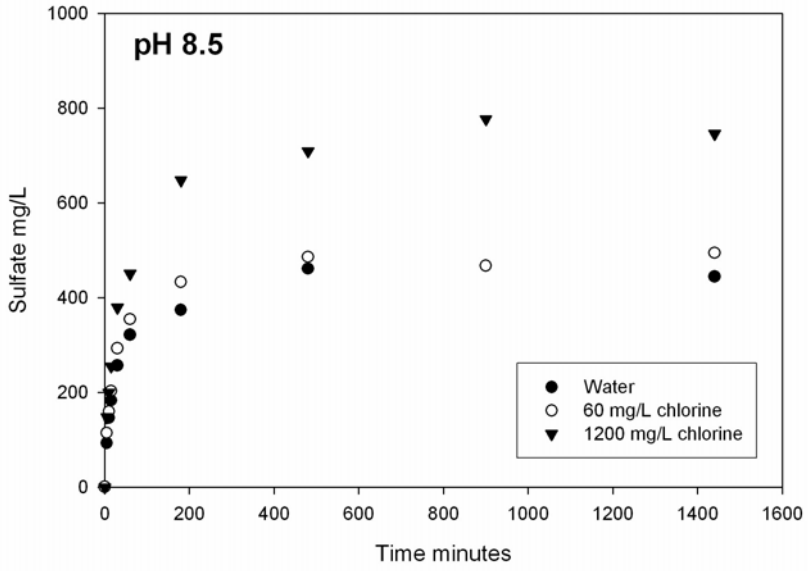

Figure 8 Sulfate concentrations measured during 24 hour exposure to chlorine solutions at pH 7.0 and pH 8.5. Highest sulfate release occurs during exposure to high dose solutions at both pH values, followed by low dose solutions, then water. Double washed (Water pre-rinse) sample experiment at pH 7.0 releases much less sulfate, indicating that soluble phases contribute considerable amounts of sulfate as washout. This could be interpreted as sulfate produced by oxidation of pyrite by oxygen in air prior to exposure to experimental solutions. In general, sulfate release is higher at pH 7.0 than at pH 8.5.

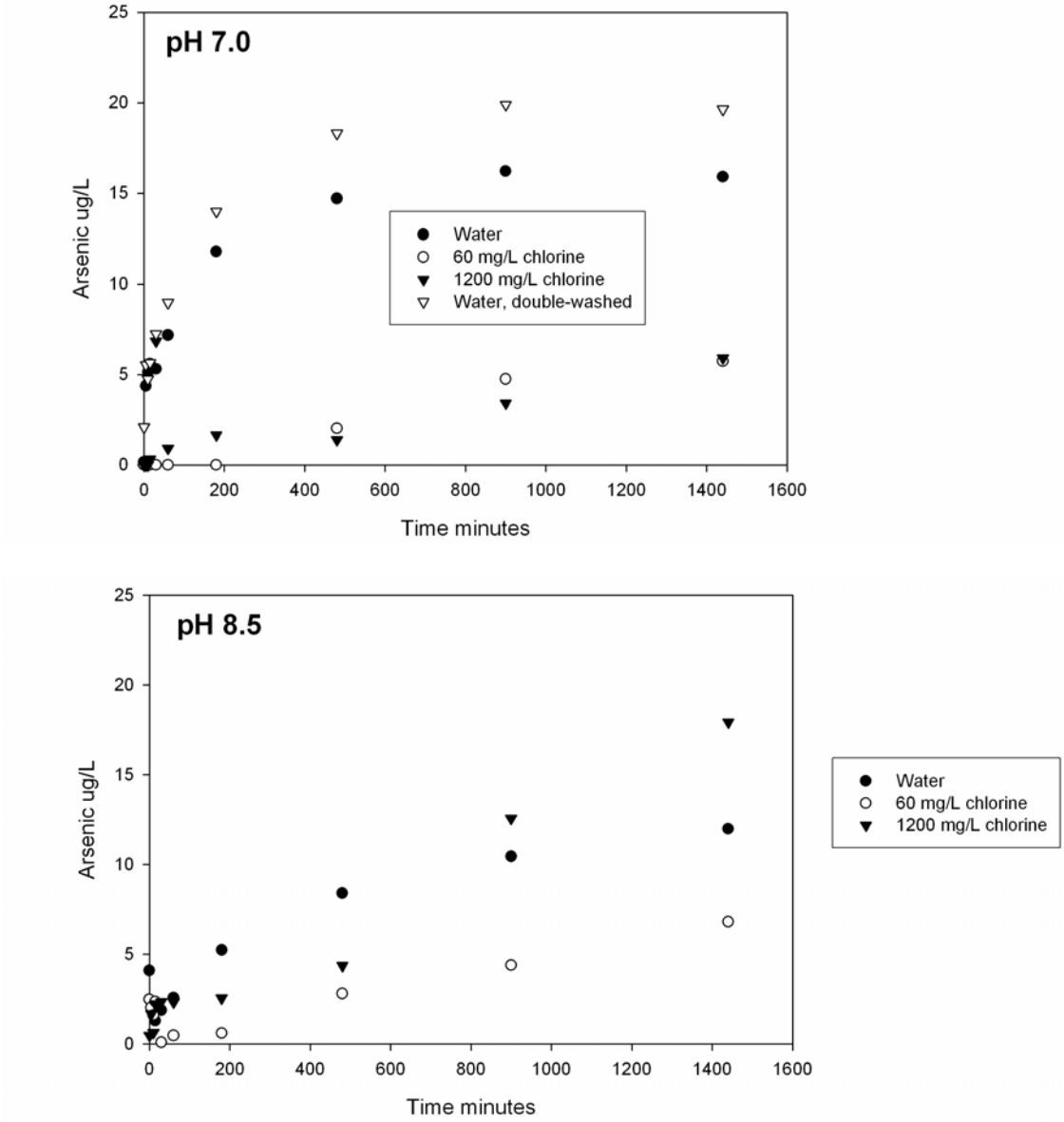

Figure 9 Arsenic (0.22 micron filtered) concentrations measured during 24 hour exposure to chlorine solutions at pH 7.0 and pH 8.5. At pH 7.0 As release is highest during water experiments. At pH 8.5 As release is highest during the high dose experiment. Arsenic release is likely highest in water due to fewer Fe-oxides forming in solution that may adsorb As, allowing more As to remain in solution. At pH 8.5, adsorption of As by Fe-oxides is impeded, allowing more of the As that is released from pyrite oxidation in the high dose experiment to remain in solution.

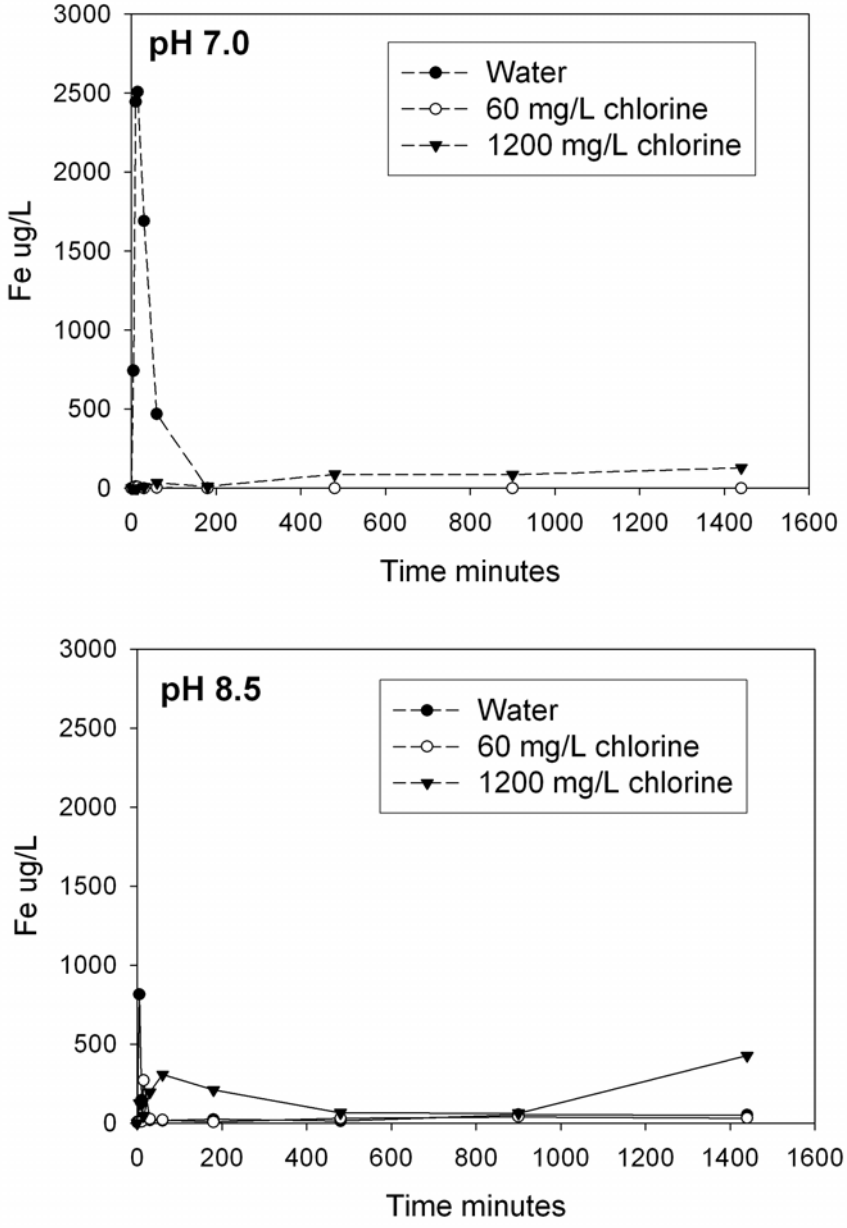

Figure 10 Iron (0.22 micron filtered) concentrations measured during 24 hour exposure to chlorine solutions. Iron concentrations in solution are very low considering a 47 wt. % abundance of Fe in pyrite. Values are low due to oxidation of ferrous iron to ferric iron and precipitation of Fe-oxides. Fe-oxides cannot pass through the 0.22 micron filter, causing low measured Fe concentrations. If precipitation did not occur, Fe values would be similar to S concentrations.

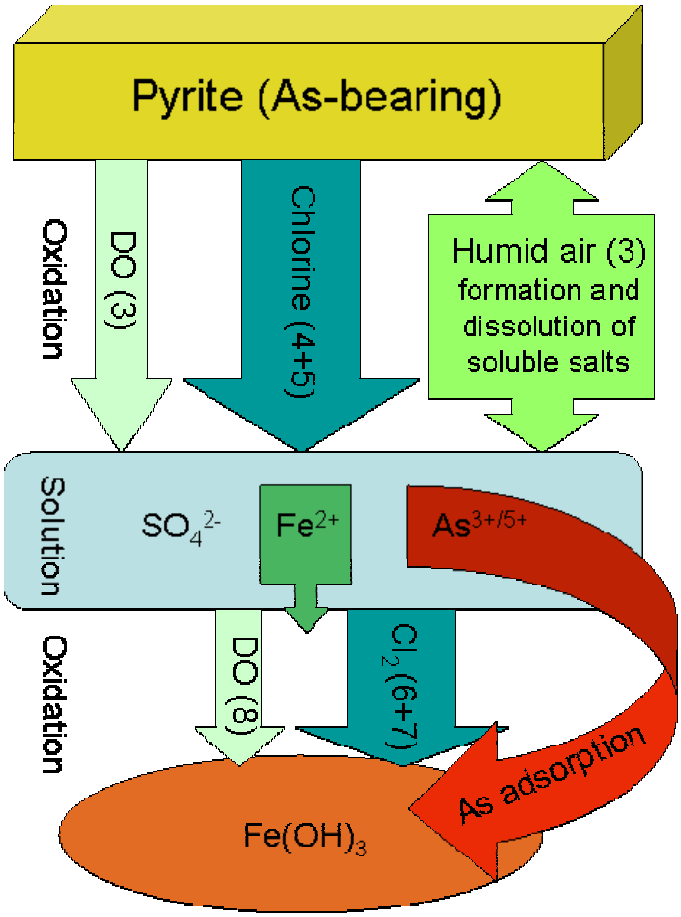

Figure 11 Summary figure of As cycling as a result of pyrite oxidation. Wide arrows represent strong oxidizing potentials. Numbers correspond to equations listed in the introduction. The three step process includes 1) As, Fe and sulfate liberation from the pyrite structure during oxidation, 2) oxidation of ferrous iron to Fe-oxides, 3) As adsorption to Fe-oxide surfaces. Note that in humid air, oxidation and salt precipitation rely on fluctuating water levels.

APPENDIX A

Results of pH 7.0 experiments

Sulfate (mg/L)

Time of Sample (minutes)	Double-Washed Water	Water	Low Dose	High Dose
0	0.22	0.19	0.50	0
5	88.23	150.21	152.22	220.17
10	117.61	219.59	218.51	362.73
15	151.65	260.08	263.47	434.71
30	212.82	343.86	351.47	562.17
60	248.28	440.16	448.11	692.39
180	304.01	524.01	551.90	837.09
480	336.10	556.94	598.70	903.84
900	344.38	584.29	617.89	901.10
1440	365.09	587.33	632.13	914.39

Arsenic (µg/L)

Time of Sample (minutes)	Double-Washed Water	Water	Low Dose	High Dose
0	1.46	0.15	0	0
5	4.37	4.36	0	0
10	4.07	5.13	0	0
15	5.32	5.59	0	0.32
30	6.61	5.31	0	6.84
60	8.67	7.17	0	0.91
180	14.74	11.80	0	1.64
480	19.04	14.70	2.02	1.39
900	25.69	16.20	4.74	3.40
1440	19.44	15.89	5.73	5.90

Iron (µg/L)

Time of Sample (minutes)	Water	Low Dose	High Dose
0	0	0	0
5	743.09	0	0
10	2444.50	9.28	0
15	2507.60	7.48	0
30	1690.25	0	7.48
60	468.44	3.27	33.92
180	0	0	11.09
480	0	0	86.81
900	0	0	85.01
1440	0	0	128.28

APPENDIX B

Results of pH 8.5 experiments

Sulfate (mg/L)

Time of Sample (minutes)	Water	Low Dose	High Dose
0	0.72	0.77	0
5	93.08	114.54	147.95
10	146.41	159.53	199.76
15	182.91	203.11	254.88
30	256.76	293.20	378.92
60	321.97	354.50	450.66
180	374.18	433.42	647.57
480	461.01	486.13	709.08
900	467.24	467.41	777.00
1440	444.82	494.85	745.97

Arsenic (µg/L)

Time of Sample (minutes)	Water	Low Dose	High Dose
0	4.1	2.49	0.48
5	2.4	2.03	1.68
10	1.99	1.61	0.65
15	1.3	2.37	2.24
30	1.89	0.1	2.36
60	2.59	0.48	2.34
180	5.24	0.61	2.56
480	8.41	2.82	4.37
900	10.46	4.4	12.57
1440	12	6.81	17.93

Iron (µg/L)

Time of Sample (minutes)	Water	Low Dose	High Dose
0	7.15	4.93	0
5	814.20	8.81	125.22
10	146.28	8.81	118.56
15	19.35	270.44	45.40
30	18.24	25.44	195.61
60	16.02	20.45	307.02
180	23.78	7.71	210.02
480	13.25	29.32	65.35
900	52.60	39.85	62.58
1440	51.49	31.54	426.75

APPENDIX C

Quantitative EPMA Analyses of pyrite in LM sections (wt. %)

No.	Fe	Cu	As	Co	Pb	Ni	S	Total
1	46.31	0	0.146	0.008	0.137	0	53.33	99.931
2	46.24	0.029	0.277	0.022	0.147	0	52.72	99.435
3	46.33	0.035	0	0.058	0.087	0.019	53.15	99.68
4	45.81	0.044	0.019	0.059	0.739	0.04	52.61	99.321
5	46.29	0	0	0.04	0.287	0	53.04	99.657
6	46.26	0	0.009	0	0.189	0.008	52.19	98.656
7	46.14	0.016	0.02	0.035	0.349	0.028	52.6	99.188
8	46.13	0	0.054	0.081	0.247	0	52.54	99.052
9	46	0	0	0.024	0.148	0	52.65	98.823
10	44.59	0	0.008	0.043	0.078	0	52.76	97.479
11	45.89	0.02	0.916	0	0.175	0	51.85	98.851
12	45.67	0.015	0.02	0.041	0.895	0	52.22	98.861
13	46.11	0	0.222	0.031	0.094	0.01	52.88	99.348
14	46.03	0	0	0.019	0.277	0	52.92	99.246
15	46.58	0.016	0	0.019	0.208	0	53.11	99.933
16	45.84	0.017	0.318	0.037	0.1	0	52.61	98.921
17	45.2	0.214	0	0.012	0.107	0.168	52.51	98.211
18	46.56	0	0.023	0.031	0.132	0	53.1	99.846
19	45.92	0.01	0	0.043	0.082	0.009	52.18	98.245
20	45.6	0.034	0.045	0.056	1.17	0.005	52.71	99.621
21	46.42	0.009	0	0.051	0.147	0	53.31	99.937
22	45.62	0.005	0.024	0.03	0.707	0.005	52.69	99.081
23	46.33	0	0	0.038	0.119	0	52.9	99.386
24	46.25	0	0	0.013	0.271	0.01	52.25	98.794
25	45.99	0	0.244	0.032	0.131	0	52.68	99.078
26	46.08	0.006	0.117	0.027	0.238	0.008	52.68	99.157
27	45.22	0.073	0.037	0.091	0.364	0.087	51.16	97.033
28	45.26	0.076	0.039	0.064	0.345	0.049	51.6	97.433
29	45.9	0.04	0.021	0.052	0.272	0.013	52.82	99.117
30	45.2	0.077	0	0.057	0.129	0.023	53.14	98.626
31	45.98	0.097	0.03	0.046	0.134	0.01	52.17	98.468
32	45.64	0.025	0.258	0.056	0.192	0.138	52.53	98.839
33	46.12	0.006	0	0.027	0.473	0.022	52.92	99.568
34	45.82	0.017	0	0.032	0.597	0.017	52.87	99.353
35	45.5	0.258	0.032	0.005	0.082	0	52.7	98.578
36	46.26	0.015	0.008	0	0.281	0	53.26	99.825
37	45.7	0.159	0	0.044	0.104	0.005	52.61	98.622
38	45.9	0.014	0	0.047	0.561	0.007	52.92	99.449
39	45.94	0	0.033	0.038	0.115	0	52.77	98.897
40	45.4	0.007	0.019	0.056	0.893	0.014	52.75	99.138
41	45.61	0.082	0	0.039	0.119	0.041	52.7	98.59
42	45.77	0.035	0	0.051	0.435	0.039	52.04	98.371
43	45.75	0.045	0.011	0	0.035	0.052	52.6	98.493
44	45.07	0.112	0.013	0.061	0.102	0.042	52.75	98.15
45	44.93	0.065	0.054	0.127	0.347	0.076	50.86	96.459
46	45.96	0.095	0.187	0.06	0.276	0.055	53.08	99.714

47	45.58	0.065	0	0.025	0.072	0.012	52.96	98.714
48	45.67	0.06	0	0.046	0.085	0.066	52.99	98.917
49	45.85	0	0	0.024	0.202	0	53.17	99.246
50	46.27	0	0.308	0.022	0.135	0.015	53.29	100.04
51	46.25	0.007	0	0.046	0.201	0	52.89	99.395
52	45.09	0.038	0	0.039	0.282	0	52.25	97.699
53	46.22	0.012	0	0.043	0.335	0	53.02	99.629
54	45.61	0.043	0.007	0.063	0.495	0.038	51.19	97.446
55	45.56	0	0.02	0.05	0.106	0	52.77	98.506
56	46.01	0.014	0.09	0.017	0.195	0	52.93	99.255
57	45.45	0.038	0	0.033	0.114	0.017	52.67	98.322
58	45.77	0.182	0	0.026	0.158	0.065	52.53	98.731
min	44.59	0	0	0	0.035	0	50.86	96.459
max	46.58	0.258	0.916	0.127	1.17	0.168	53.33	100.04
ave	45.835	0.038	0.063	0.039	0.267	0.021	52.640	98.903